JOURNAL OF PROPULSION AND POWER
Vol. 27, No. 2, March–April 2011

Electrospray Propulsion Based on Emitters Microfabricated in Porous Metals

Robert S. Legge, Jr.* and Paulo C. Lozano†
Massachusetts Institute of Technology, Cambridge, Massachusetts 02139

DOI: 10.2514/1.50037

Performance of microfabricated porous metal electrospray emitters is examined for a number of ionic liquid propellants and emitter clustering configurations. A method of creating dense arrays of miniaturized emitters using electrochemical etching microfabrication techniques is presented. Time-of-flight mass spectrometry and direct current measurements are used to characterize the emission of single emitters with four ionic liquids of different physical properties. Pure ion emission is observed for all ionic liquids tested. Results indicate that ionic liquids with lower ion masses produce more thrust at a given voltage than liquids with heavy ions due to a significant reduction in emitted ion current for the heaviest ions, likely caused by a combination of increased hydraulic resistance and slower charge relaxation times, respectively, due to higher viscosity and lower electric conductivity. Experiments with varying linear emitter array densities show that the current produced by individual emitters remains fairly constant, indicating that the thrust density can be increased with emitter miniaturization and clustering. A two-dimensional emitter array is constructed from three linear arrays and experiments show that the device produces an average current of around 1 μA per emitter at the highest voltages. Direct thrust measurements using a torsional balance show that the test fixture produces between 0.05 to 0.1 μN of thrust per emitter, as anticipated by theoretical estimates.

Nomenclature

$\tilde{A}$	=	specific area, m^2/N
d	=	emitter separation, m
f	=	current fraction
I_{SP}	=	specific impulse, s
L	=	time-of-flight distance, m
m	=	ion mass, kg
$\dot{m}$	=	mass flow rate, kg/s
$\tilde{m}$	=	specific mass, kg/N
N	=	grid number
N_E	=	number of emitters
n	=	degree of solvation
q	=	charge, C
r_c	=	radius of curvature, m
T	=	thrust, N
$\tilde{V}$	=	specific volume, m^3/N
V	=	accelerating voltage, V
v	=	velocity, m/s
α	=	thruster frame factor
β	=	porosity fraction
Δt	=	time-of-flight, s
γ	=	surface tension, N/m
δ	=	emitter to extractor distance, m
ε_0	=	permittivity of free space, F/m
ξ	=	thruster scaling factor
η_P	=	polydispersive efficiency
κ	=	conductivity, Si/m
μ	=	viscosity, cP
Φ_B	=	beam potential, V
ρ	=	density, kg/m^3

Received 24 March 2010; revision received 9 September 2010; accepted for publication 9 October 2010.

*Graduate Student, Department of Aeronautics and Astronautics; Presently, MIT Lincoln Laboratory.

†Associate Professor, Department of Aeronautics and Astronautics, 70 Vassar Street. Member AIAA.

I. Introduction

ELECTROSPRAY propulsion is based on the electrostatic extraction and acceleration of charged particles from a liquid surface to produce thrust for spacecraft. Electrospray devices share a number of characteristics that differentiate them from other electric propulsion devices. The fundamental working mechanism is based on a process by which a conductive liquid surface is deformed under the influence of an electric field applied between a liquid meniscus, traditionally held at the tip of a sharp needle-shaped emitter, and a downstream circular aperture. This phenomenon was studied by G.I. Taylor [1] for a perfect conductor, infinite in size, surrounded by charge free space. Under such conditions, the liquid deforms into a conical shaped structure. In Taylor's analysis, the internal half angle of the cone is found to be a constant (49.29°) independent of the applied voltage or the physical properties of the liquid. It has been experimentally determined that even liquid cones with finite conductivities and sizes deform into structures that closely match Taylor's predictions. In general, the electric field E is balanced by surface tension σ at any point r measured from the apex of the cone. This requires the electric field to intensify as the inverse of the square root of r, thus becoming extraordinarily large near the cone apex. The apparent singularity is resolved by the emission of charged particles from the cone apex. The nature of this emission depends heavily on the properties of the liquid. It is observed that organic solutions (e.g., glycerol, formamide, water, etc.) doped with inorganic salts (e.g., NaCl, KBr, NaI, etc.), will produce a liquid jet which is convected away from the Taylor cone apex, eventually breaking up into a fine spray of charged droplets. If the conductivity is high and the flow rate is low (high κ/Q), it becomes possible to field-evaporate solvated ions directly from the liquid surface. This typically occurs near the cone-to-jet transition region where the electric field is most intense. In contrast, with liquid metals it is possible to suppress the jet completely as the field becomes large enough to produce direct metallic ion evaporation. A third scenario exists when the liquid is a room temperature molten salt, also known as an ionic liquid. In this case, depending on the liquid supply rate, it is possible to change the operation mode from a droplet dominated emission mode to a pure ion emission regime [2]. This transition is not observed in organic solutions and appears to be unique to ionic liquids. In ionic liquid ion sources (ILIS), for an ionic compound of the generic form $[A+][B-]$, the ions emitted are of the type $[AB]_n[A+]$ in the positive polarity and $[AB]_n[B-]$ in the negative polarity. The degrees of solvation (n) are typically 0 (monomer), 1 (dimer) and, to less extent, 2 (trimer).

Higher values of n are sometimes observed with very low intensities and do not contribute in a practical way to the performance of a thruster. These ions exhibit narrow energy distributions and little losses, allowing thrusters operating in the pure ionic regime to work with a wide range of specific impulses at efficiencies around 80%.

Electrospray thrusters are considered *micropropulsion* devices due to the low forces delivered per Taylor cone. They are ideal for applications where exceptionally accurate and stable thrust is required, such as the LISA (laser interferometer space antenna) mission and other formation flight missions. To be used as main propulsion, including attitude control, individual emitters need to be miniaturized and clustered in dense arrays operating in parallel. This fact was acknowledged early in the development of Colloid Thrusters [3,4], although it was technologically difficult at the time to both miniaturize and precisely align emitter arrays. Recent advances in micromanufacturing techniques enable the fabrication of emitter arrays with the required characteristics. Electrospray thrusters now have the potential to be competitive with plasma-based ion engines in terms of thrust (area) density. Furthermore, direct ionization is not required in ILIS, eliminating the need of dc or RF cathodes and magnetic circuits and the propellant itself is a zero-vapor pressure dense liquid that can be easily and compactly stored in space with minimal, or possibly no pressurization. Because of this, fully micromachined electrospray thrusters would display compactness features difficult to match by current low/medium power level plasma thrusters. In all likelihood, the immediate beneficiaries of electrospray propulsion would be small, power-limited satellites.

In ILIS, the ionic liquid propellant is supplied to the emitter tip by passive capillary forces as needed by the ion field evaporation process. The main challenge in making ILIS devices is the microfabrication of the emitters. Three emitter technologies have been studied to date: externally wetted needle emitters, externally wetted silicon emitters and porous metal emitters. Externally wetted needle emitters are fabricated by first electrochemically etching tungsten wire to produce sharpened emitters with a tip radius of curvature of 10–100 μm. Several additional steps are required to etch grooves on the surface to aid in the fluid transport along the emitter. The emitters have been shown to operate in the pure ionic regime with emission of a few hundred nA of high quality beams displaying narrow energy and angular distributions at room temperature with several ionic liquids [5]. Experiments with ionic liquids composed of significantly heavier ions also produce high quality ions beams, although they tend to have comparatively smaller emission currents on the order of tens of nA [6,7], and therefore lower thrust. The fabrication process of emitter arrays using this configuration was not considered due to difficulties in clustering individual emitters at the microscale. Instead, externally wetted emitters were microfabricated in silicon using well known and developed techniques at the required scales. However, wetting of silicon by the ionic liquids is poor and despite ad-hoc surface treatments that promote hydrophilicity, the emission currents per emitter are in general lower than ILIS emitters [8]. Furthermore, liquid delivery to the artificially roughened silicon surface is not straightforward and requires some form of active pumping. In contrast, porous metal emitters increase the fluid transport capacity through the emitter and towards the ion emission sites by opening up internal fluid routes. Similar to externally wetted ILIS, porous metal emitters operate in the pure ionic regime at room temperature, albeit at much larger current levels, likely due to the increase in fluid transport provided by the emitter porosity.

This paper first describes the operational characteristics of a single porous metal emitter for different ionic liquid propellants with varying physical properties. The performance of linear (one-dimensional) emitter arrays is then investigated to determine the effect of emitter separation on operational performance. Finally, the performance of a two-dimensional array is presented together with efforts to miniaturize high-density porous metal arrays. In this work we only investigate a single emitter material due to a very specific masking technique we developed for tungsten, and a single porosity due to material availability. Preliminary results with porous Nickel emitters are presented elsewhere [9].

II. Electrospray Thruster Scaling

One of the most important challenges in the space industry today is to increase spacecraft functionality and capabilities with minimal costs. To accomplish this goal, there has been a wave of research and development of spacecraft in the 1–100 kg class with significant operational capability, but with limited propulsive options. Most spacecraft systems (electronics, communications, payloads, etc.) are amenable to direct miniaturization, but propulsive systems pose problems. Existing technologies, including monopropellant, bipropellant, and cold gas systems require pressurized propellant storage and complex, reliable fluid management actuators which are difficult to scale without drastically reducing the overall propellant mass fraction of the system, and consequently the overall ΔV. In addition, the miniaturization of combustion chambers leads to a direct loss in performance due to relatively low adiabatic flame temperatures required to curb the correspondingly large heat transfer to chamber walls. Typical electric propulsion systems that require gas phase ionization of propellant have proven to be difficult to miniaturize without a serious impact in efficiency and lifetime due to the required increase of plasma density [10].

Given that the thrust produced by a single ILIS emitter is on the order of 100 nN, many missions would require clustering of emitters to meet typical thrust requirements. The ability to scale a two-dimensional array of ILIS emitters can be quantified by the propulsion system footprint on a spacecraft, which is defined here in terms of the device area, volume and mass per unit thrust. Figure 1 shows the representative geometry of a two-dimensional ILIS array with emitters spaced out (triangular arrangement) by a distance d. Assuming that each emitter produces the same thrust T, the specific (per unit thrust) area is a function of the emitter spacing geometry and the additional area caused by thruster packaging. For a triangular arrangement of emitters, with a separation between neighboring emitters d, the area taken by a single emitter is given as:

$$A = \alpha_1 \frac{\sqrt{3}d^2}{2}$$

where α_1 is a factor which accounts for the increase in area caused by the thruster packaging. For large arrays with a small frame, this factor tends to be small. As an example, for our current efforts at producing two-dimensional arrays, the packaging adds roughly 30% to the total thruster footprint, making the factor equal to 1.3. The specific area is then given by:

$$\tilde{A} = \alpha_1 \frac{\sqrt{3}d^2}{2T}$$

The specific volume of the thruster can then be approximated by the specific area multiplied by the depth of the thruster. The depth of the thruster is a function of the emitter length, the grid thickness and spacing and the depth of the frame, which will also be treated as an additional multiplicative factor of 3, which is consistent with current two-dimensional array fabrication efforts. Additionally, the number of grids in the thruster is represented by N_G. The specific volume is then given as:

$$\tilde{V} = \alpha_2 \tilde{A} d[N_G(\xi_G + \xi_S) + \xi_E]$$

where the variable ξ is the ratio of various component dimensions to the emitter spacing d, and accounts for the overall scaling effect of miniaturization in terms of the emitter spacing. The subscripts G, E, F, and S stand for grid, emitter, frame and grid spacing, respectively. The specific mass is given by:

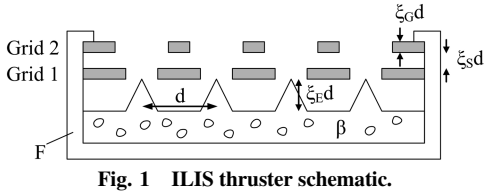

Fig. 1 ILIS thruster schematic.

Table 1 Expected operational and geometric characteristics of a typical ILIS thruster

α_1	1.3	ρ_G	2.3 g/cm^3
α_2	3	ρ_E [W]	19.3 g/cm^3
N_G	2	ρ_E [Ni]	8.9 g/cm^3
ξ_G	0.7	ρ_F	2.7 g/cm^3
ξ_S	3.3	β	0.2
ξ_E	0.8	T	0.1 μN

Table 2 ILIS footprint in terms of mass, volume and area compared with those of existing electric propulsion technologies. Smaller footprints are always desirable in space propulsion devices

Thruster	d, μm	$\tilde{m}$, g/mN	$\tilde{V}$, cm^3/mN	$\tilde{A}$, cm^2/mN
Tungsten ILIS array	300	8.33	8.03	10.13
	100	0.31	0.30	1.13
Nickel ILIS array	300	6.32	——	——
	100	0.23	——	——
Typical ion engine		91	109	7.7
Low-power Hall thruster		156.3	63	6.25

$$\tilde{m} = \tilde{A}d[N_G\rho_G\xi_G + \rho_E\xi_E(1-\beta) + \rho_F(N_G\xi_G + \xi_E)(\alpha_2 - 1)]$$

where the porosity (fraction of the material that is empty space) of the emitter is represented as β. As an example of the expected footprint metrics of an ILIS thruster, a theoretical two-dimensional emitter array has been configured with the characteristics given in Table 1. The extractor thickness is limited by beam divergence and electrostatic field deformation as well as manufacturability, however, this work does not attempt optimization in this respect and the extractor thickness was selected to guarantee little or no beam interception. A comparison of the footprints for such an ILIS device for emitter separations of 100 and 300 μm and some typical footprints of existing low-power electric propulsion devices are shown in Table 2. The 100–300 μm range is selected for comparison since this is the immediate goal for our thrusters and is within the expected manufacturing capabilities of our process. Smaller emitter separations are possible, although they are more challenging to implement and are reserved for future work. Additionally, while current emitters are fabricated from tungsten, lighter metals could be used to reduce thruster mass. The results demonstrate that the 300 μm ILIS emitter arrays show significant reductions in the overall mass and specific volume over traditional electric thruster technologies, while the 100 μm ILIS emitter arrays show even more dramatic reductions in all three thruster footprints with the specific mass and specific volume being orders of magnitude lower. The dramatic reduction in the volume and mass footprints enables ILIS emitter arrays to be used for two technologically challenging areas that current electric propulsion technologies do not satisfy, including use on pico and nano satellites, and in the concept of thin thruster panels which are similar in nature to solar panels since they can be directly sized to fit the needs of the spacecraft.

In addition to the benefits of having a small footprint, ILIS devices also have an intrinsic ability to be scaled to meet the needs of a wide variety of spacecraft. The smallest thrust achievable for an ILIS device is simply the thrust of a single emitter, which can be on the order of a few nN, while the maximum amount of thrust achievable has the potential to surpass that of low-power plasma thrusters given the large thrust density of densely packed electrospray emitters. Miniaturized electrospray arrays also have the potential of being less affected by space charge saturation. The ratio of the space charge limited current of an electrospray (ES) device to a traditional ion engine (ion) is a function of the accelerating voltage V and the grid spacing D (for ILIS thruster this is the emitter to extractor distance), and can be approximated using Child–Langmuir's law:

$$\frac{J_{\mathrm{ES}}}{J_{\mathrm{ion}}} \approx \left(\frac{V_{\mathrm{ES}}}{V_{\mathrm{ion}}}\right)^{3/2}\left(\frac{D_{\mathrm{ion}}}{D_{\mathrm{ES}}}\right)^{2}$$

The characteristic emitter to extractor spacing in electrospray devices can be precisely controlled using microfabrication techniques, and therefore can be much smaller than the traditional ion engine grid spacing operating at similar voltages. Grid spacings of microfabricated electrospray devices in the 20–200 μm range would yield, respectively, space charge limiting currents 2500 –25 times higher than a traditional ion engine with typical 1 mm grid spacing.

III. Experimental

A. Porous Metal Emitter Fabrication

Porous metal electrospray emitters of various geometries are microfabricated using electrochemical etching controlled through the use of a polyimide mask. Mask patterning was carried out in a class 10,000 clean room at the MIT Microsystems Technology Laboratories while emitter etching was conducted at the MIT Space Propulsion Laboratory. Figure 2 shows the main steps in the fabrication process [11] which can be used to create single emitters as well as arrays of multiple emitters. First, porous tungsten samples of 0.5 μm pore size obtained from American Elements, Los Angeles, CA, are cut into small pieces using a Disco Abrasive System Model DAD-2H/6T diesaw. The sample is then filled with Shipley 1827 positive photoresist using a surface puddle technique and then spincasted at 2000 rpm for 40 s to create a thin and uniform surface layer of 5 μm. The sample is then heated in an oven to harden the photoresist by driving off solvents.

Following the photoresist application and hardening, all surfaces of the sample are then exposed with UV light in a Karl Suss MJB3 photomask aligner to break down the photoresist structure on the surfaces to allow removal in Microposit MF-319 (Rohm–Haas) developer. At this point the surface of the porous tungsten sample is clean while the porosity is filled with photoresist. Next, a 2–3 μm layer of PI-2556 polyimide (HD Microsystems) is applied to one side of the sample using the puddle and spincast technique at 500 rpm for 15 s and then 1500 rpm for 45 s, and is prebaked to drive off solvents (Step 2). Polyimide was chosen as the electrochemical etch masking material for its good resistance to sodium hydroxide

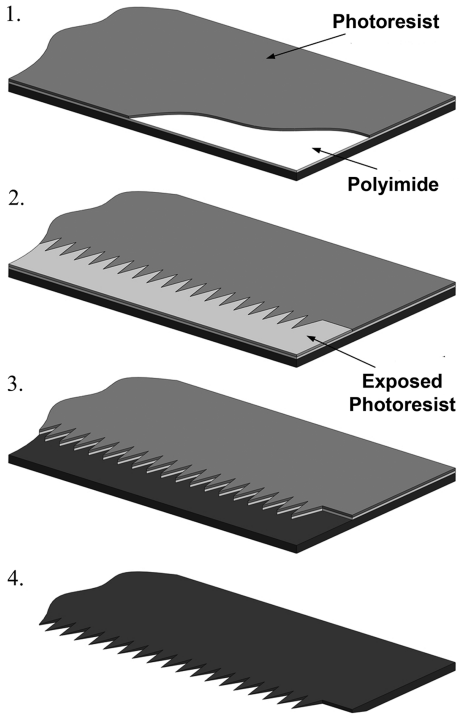

Fig. 2 Fabrication process steps.

[12] and ability to be precisely patterned using standard photolithography techniques.

After the initial polyimide curing, a second 5 μm layer of Shipley 1827 positive photoresist is applied on top of the polyimide, using the puddle and spincast technique (Step 1). The top layer of photoresist is then patterned by selective UV light exposure through a transparency mask containing the intended emitter geometry (Step 2). The sample is then developed in Microposit MF-319 developer to remove the exposed photoresist areas and to etch the underlying polyimide, thereby transferring the pattern from the photoresist to the polyimide (Step 3). Acetone is then used to remove the photoresist from the surface and bulk of the sample.

Following the photoresist removal, the polyimide is cured in an oven to harden it against the electrochemical etch chemistry. The sample is then electrochemically etched in a 1 N sodium hydroxide solution, using stainless steel as cathode material, until the excess tungsten is removed and the emitter geometry is formed. The polyimide masking layer is then removed in a piranha acid bath consisting of a 4:1 H_2SO_4 and H_2O_2 mixture and the emitters are complete (Step 4).

B. Apparatus

The characteristics of electrospray emission are measured under vacuum at pressures less than 10^{-6} torr to avoid significant neutral particle interactions. The vacuum tank consists of a cylindrical chamber with an inner diameter of 197 mm and length 495 mm. A stainless steel extension with an inner diameter of 56 mm and a length of 365 mm is installed to increase the resolution of the time-of-flight experiments. Roughing is provided by a Varian SD-40 mechanical pump while two Varian V-70 turbo pumps are used to ultimately reach the lowest pressures. Chamber pressure is monitored using a Varian ionization gauge controlled by a Varian multiguage. A Matsusada AMS-5B6 bipolar high voltage power supply provides the extraction voltage difference between the emitter and the grounded extractor electrode. The power supply is capable of fast polarity switching and is controlled by an Agilent 33220A function generator controlled by LabView.

Voltage steps of various amplitudes are applied between the emitter and the extractor to measure the amount of emitted current as a function of voltage. Figure 3 shows both a sample experimental applied voltage profile and the resulting emitted current for a linear emitter array. The voltage profile alternated polarities to eliminate the possibility of detrimental electrochemical reactions between the ionic liquid and the tungsten substrate [13]. The emitted current response to a single voltage step is shown in Fig. 4. For each step, the amount of current is highest at the start when the concentration near the ion evaporation site is the highest. This initial behavior is transient in nature and the current quickly reduces to a stable level where current data is taken. To reduce experimental error, the current values are averaged for the duration of the step after the initial transient. The variation of the current in this region is typically less than 5%.

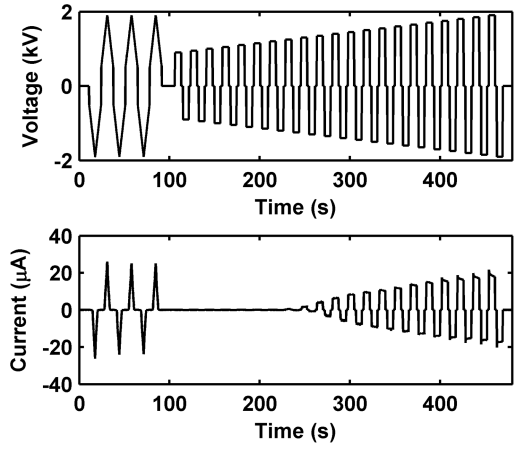

Fig. 3 Sample voltage profile (top) and the resulting current (bottom) with a 0.06 Hz alternation frequency.

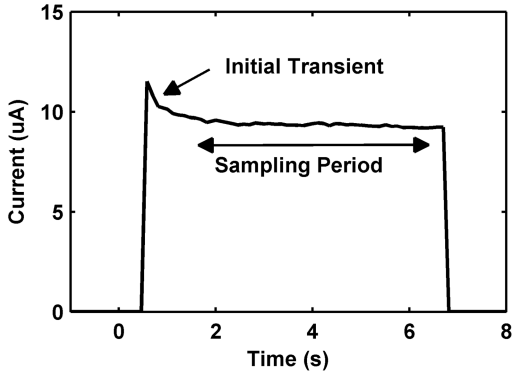

Fig. 4 Current response during a single extractor voltage step.

Time-of-flight (TOF) mass spectrometry is used to determine the composition of the emitted current. The single gate time-of-flight setup has been described in detail elsewhere [14,15] and is schematically shown in Fig. 5. Briefly, the emitter assembly is aligned to the entrance of a three electrode Einzel lens, which provides beam collimation with a focusing voltage close to the extraction voltage. Immediately downstream from the lens is an electrostatic gate composed of interleaved wires controlled by a BNC-555 pulse generator. When the gate is turned on, a high-speed amplifier biases the grids to ± 900 V, and the beam is deflected so that no current reaches the collector plate, located a distance of 750–765 mm away. The collector is composed of a 38 mm diameter metallic plate, and the collected signals are amplified through a noninverting amplifier based on the MAX477 op-amp and captured by an Agilent Oscilloscope. Secondary electron emission at the collector plate is suppressed by a grid biased to -50 V just before the plate. Errors in the time-of-flight measurement are caused by uncertainty in the measurement of the flight distance as well as uncertainty in the interpretation of the flight time due to widening of the signal caused by both the physical time spread of the ion signal (due to energy spreads) and spreads introduced by the amplifier electronics. Once a consistent interpretation for the time-of-flight is made from the signal, physical error in the actual flight times are small since each TOF spectrum is averaged from a large number (>256) of waves, displaying negligible variance. In this work, the interpretation of the time-of-flight is taken when the current in the TOF spectra steps decreases by 5% from its nominal value.

Direct thrust measurements were conducted at the Busek Company, Natick, MA using a torsional balance capable of measuring submicronewton forces [16]. The torsional balance uses flexural pivots and electrostatic forces for both active damping and calibration.

C. Thruster Parameters

In time-of-flight experiments, high-speed electronics characterize the rate at which charged particles travel a known distance, L. The specific charge q/m is calculated from the measured flight time Δt

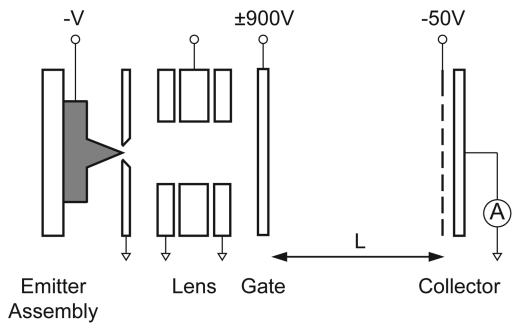

Fig. 5 Time-of-flight experimental setup.

assuming the beam potential ϕ_B is known. Applying energy conservation

$$\left(\frac{q}{m}\right) = \frac{(L/\Delta t)^2}{2\phi_B} \tag{1}$$

Previous work has shown that the applied voltage V approximates the beam potential to within 99% [15], therefore allowing the use of V in the previous expression in the absence of direct beam energy measurements. The mass corresponding to each observed species is then easily found as a function of the ion charge. Typically, the electric fields required for field ionization are about an order of magnitude larger than those required for field evaporation in ionic liquids. In field ionization, a substance typically a gas from a source or evaporated from a substrate is ionized when passing through a region of high electric field. Field ionization processes frequently produce a population of singly and multicharged ions. In ion evaporation, ions located at the surface of the substrate are directly extracted, and since the work required is typically lower than ionization potentials, practically all ions evaporated are singly charged, therefore $q = e$

$$m = \frac{2eV}{(L/\Delta t)^2} \tag{2}$$

Propulsive parameters including the mass flow rate, specific impulse, thrust and polydispersive efficiency can then be estimated following the identification of the beam composition. The polydispersive efficiency is a measure of the inefficiency caused by emitting species with dissimilar specific charges and is a good indicator of the upper bound for thruster efficiency [17]. Additional losses, including beam interception by extraction or acceleration electrodes, beam angular spreading, energy losses and ion fragmentation during acceleration are typically small for some ionic liquids, and in principle could be controlled by design and proper operating conditions [8,17]. The mass flow rate for each species is estimated as the total amount of current emitted by each species divided by the corresponding charge to mass ratio

$$\dot{m} = I_{\text{tot}} \cdot \sum_i \frac{f_i}{(q/m)_i} \tag{3}$$

The thrust and specific impulse are then computed from the experimental time-of-flight as:

$$T = \sum_i \dot{m}_i c_i \tag{4}$$

$$T = \sum_i \dot{m}_i (L/\Delta t)_i \tag{5}$$

$$I_{\text{SP}} = T/\dot{m}g \tag{6}$$

The estimated polydispersive efficiency [17] considering only the monomer and dimer contributions is a function of the specific charge ratio of the monomer to dimmer and the monomer to total current fraction:

$$\eta_p = \frac{[1-(1-\sqrt{\lambda})f_0]^2}{1-(1-\lambda)f_0} \tag{7}$$

where

$$\lambda = \frac{(q/m)_2}{(q/m)_1} \qquad f_{N_G=0} = \frac{I_0}{I_0 + I_1} \tag{8}$$

and where I_0 is the monomer current and I_1 is the dimer current.

IV. Single Porous Emitter Results

A. Emitter Characterization

A single emitter was tested with several ionic liquids of increasing ion mass to characterize the effect on thrust produced per emitter. A porous metal emitter of 0.5 μm average pore size was fabricated using the microfabrication process explained previously. The emitter, shown in Fig. 6, has a length of 2.14 mm, a base width of 1.196 mm, an emitter thickness of 600 μm and a tip radius of curvature of 8.25 and 9.77 μm in the two principal directions, giving an effective tip radius of curvature of 4.47 μm.

The porous metal emitter was characterized with four ionic liquids of differing physical properties including: ion mass, surface tension, density, electrical conductivity and viscosity, shown in Table 3. The ionic liquids in order of increasing ion mass are: EMI-BF_4 (1-ethyl-3-methylimidazolium tetrafluoroborate), EMI-Im (1-ethyl-3-methylimidazolium bis(trifluoromethylsulfonyl)imide), EMI-Beti (1-ethy-l3-methylimidazolium bis(pentafluoroethyl) sulfonylimide), and $C_5MI-(C_2F_5)_3PF_3$ (1-pentyl-3-methylimidazolium tris(pentafluoroethyl) trifluorophosphate), referred to as MPI. Except for EMI-BF4, these substances are considered as poor ionic liquids since pure ion emission cannot be obtained at room temperature using conventional capillary emitters. However, as shown here, the pure ionic mode is achievable for these heavy liquids using porous metal emitters. By heavy, we mean ion masses larger than typical atomic masses.

The eight subplots displayed in Fig. 7 show the time-of-flight spectra obtained for the four ionic liquids tested in each polarity. The plots on the left show the collected current as a function of species mass, where the mass was found from the flight time using Eq. (2). The vertical lines show the mass values corresponding to the expected emitted ion species which include the monomer, the dimer as well as the trimer for some liquids. The plots on the right show the collected current as a function of time showing that the emitters operate in the pure ion regime with no observed droplets for any of the ionic liquids. The results closely agree with previous time-of-flight experiments with EMI-BF_4 in both cylindrical needle emitters [14] and with arrays of ribbonlike emitters [20]. Table 4 gives more detailed data collected during the TOF experiment including: the time-of-flight, the species velocity, the beam potential, and the

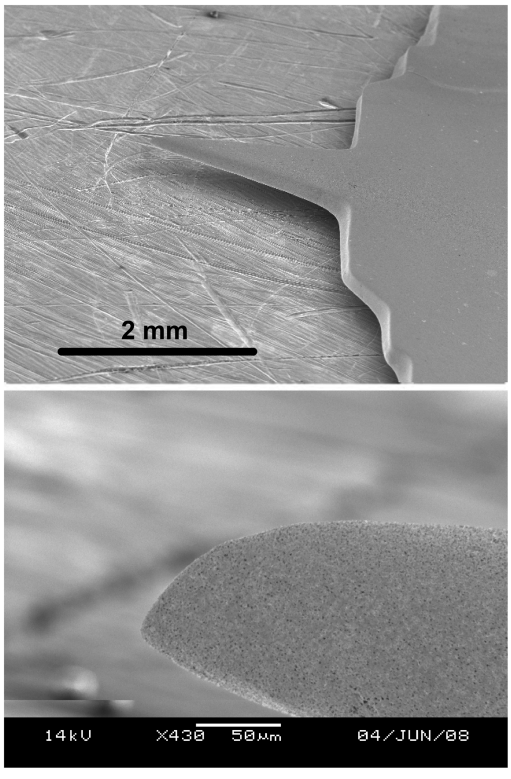

Fig. 6 Single porous metal emitter.

Table 3 Properties of the ionic liquids tested at 273 K

Ionic liquid	m^+, amu	m^-, amu	γ, dyn/cm	ρ, kg/m^3	κ, Si/m	μ, cP
EMI-BF_4 [18]	111.2	86.8	45.2	1240	1.4	38
EMI-IM [19]	111.2	280.2	41	1517	0.84	43
EMI-Beti [7]	111.2	380.15	28.75	1600	0.34	61
MPI [7]	153.24	445.01	30.33	1590	0.16–0.229	140

calculated ion mass. The time-of-flight is experimentally measured, while the ion velocity is computed from the experimental time-of-flight and the flight distance, and the current fractions are measured by averaging the relative magnitudes of the respective current steps.

Since the goal of the time-of-flight measurement is to identify the composition of the ion beam, for each ionic liquid, the flight distance was adjusted to make the singly charged positive ion have the correct mass. This flight distance was then used in the mass calculations for

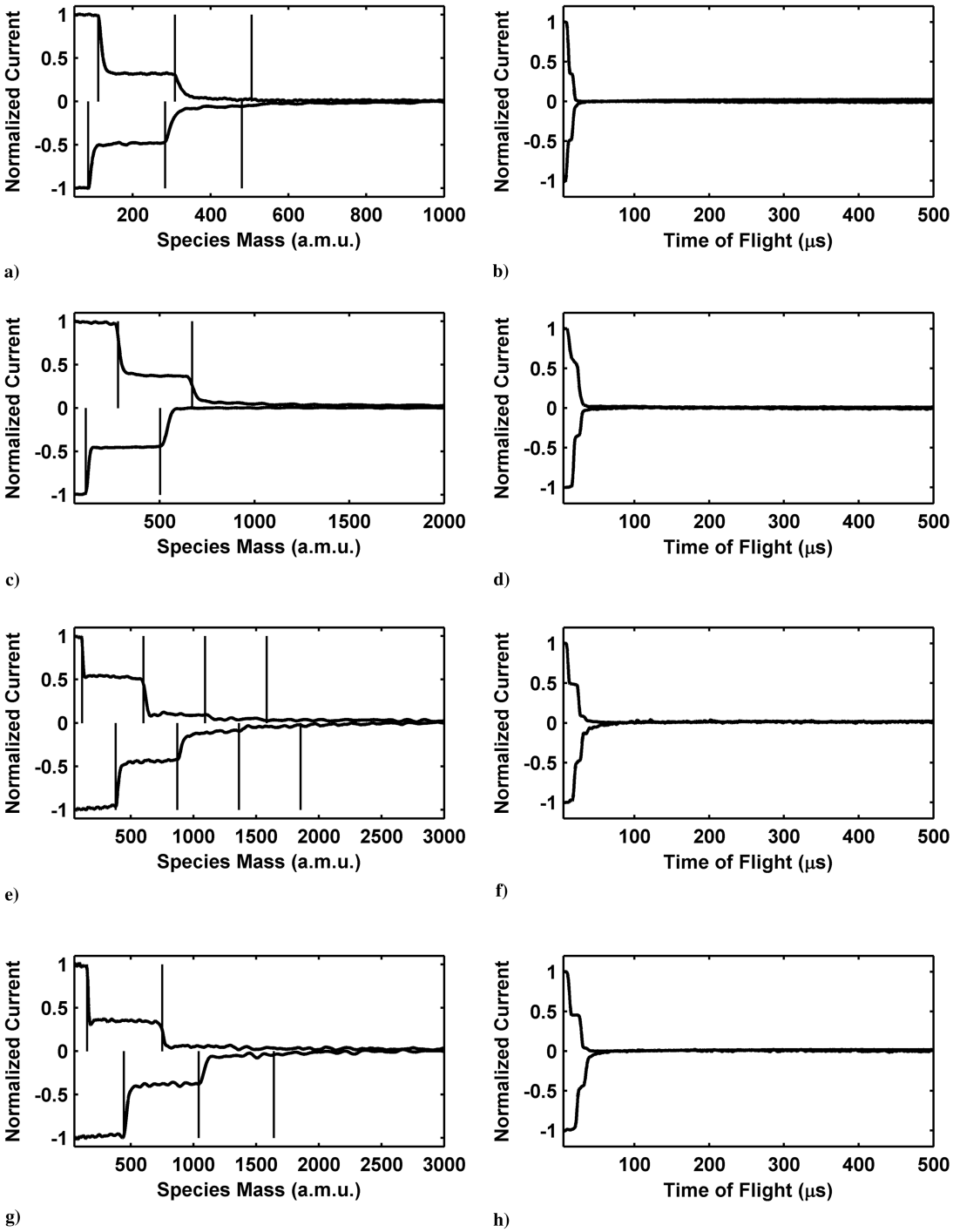

Fig. 7 Time-of-flight results for the ionic liquids EMI-BF_4 (subplot a, b), EMI-IM (subplot c, d), EMI-Beti (subplot e, f), and MPI (subplot g, h). On the left, the normalized current is plotted as a function of species mass as given by Eq. (2). Note that the *x*-axis is not equal for the different ionic liquids due to differences in ion mass. On the right, the normalized current is plotted versus time showing that all liquids are being emitted in the pure ionic regime with no droplets.

Table 4 Time-of-flight results for the four ionic liquids tested showing some measured quantities including: the time-of-flight, the species velocity, the beam potential, the calculated ion mass, and the species contribution to the total collected current. The fractional difference between the experimentally calculated ion mass and the actual species mass is shown to be on the order of a few percent

		Experimental					Exact	
Polarity	n	Δt, μs	v, km/s	$V-\Delta V$, eV	m, amu	f, %	m_E, amu	$1-m_E/m$, %
EMI-BF_4								
Positive	0	11.33	67.53	2580	111.2	68.5	111.2	——
	1	18.87	40.55	2580	308.5	29.0	308.4	−0.02
Negative	0	9.83	77.84	2700	87.6	52.7	86.0	−1.86
	1	17.67	43.30	2700	283.0	42.6	283.2	0.05
	2	23.27	32.88	2700	490.9	4.8	480.4	−2.18
EMI-IM								
Positive	0	11.5	65.60	2480	111.2	53.9	111.2	□
	1	24.5	30.79	2480	504.7	45.6	502.6	−0.42
Negative	0	18.1	41.68	2400	266.6	64.1	280.2	4.86
	1	28.2	26.75	2400	647.1	33	671.6	3.65
EMI-Beti								
Positive	0	11.8	62.90	2280	111.2	47.6	111.2	——
	1	27.6	26.89	2280	608.4	46.2	602.5	−0.96
	2	38.1	19.48	2280	1159.3	4	1093.9	−5.98
	3	45.0	16.49	2280	1617.2	1.8	1585.2	−2.02
Negative	0	19.9	37.30	2900	402.3	55.5	380.2	−5.82
	1	30.0	24.74	2900	914.2	33.4	871.5	−4.90
	2	37.7	19.69	2900	1443.7	6.4	1363	−5.92
MPI								
Positive	0	12.3	60.43	2900	153.2	66.3	153.2	——
	1	27.4	27.53	2900	738.2	31.0	751.5	1.77
	2	37.3	20.23	2900	1368.0	2.2	1349.7	−1.35
Negative	0	22.7	32.74	2580	464.3	58.1	445.0	−4.34
	1	35.2	21.12	2580	1116.5	31.0	1043.3	−7.02
	2	42.9	17.59	2580	1609.9	6.1	1641.5	1.93

the remaining species for the given ionic liquid and is then compared with the actual expected species mass enabling a coarse measurement of experimental error that is on the order of a few percent. The calculation of the ion mass requires knowledge of the beam potential. Extracting the precise beam energy from these measurements lacks accuracy given the resolving power of the TOF apparatus. Because of this, the beam potential has been assumed to be 10 V lower than the accelerating voltage, which is consistent with previous measurements using a retarding potential analyzer [15].

The current emitted as a function of applied voltage was also measured at room temperature (20°C) and is shown in Fig. 8. As the average mass of the ionic liquid increases, the amount of current emitted decreases. It is important to note that the current emitted by the porous emitter far surpasses that shown to be emitted from externally wetted needle emitters, particularly for heavy ionic liquids [7]. For example, Larriba et al. showed that an externally wetted emitter produced between 10 and 12 nA of beam current with MPI [7] while the porous metal emitters produce a 20 fold increase of over 200 nA. This substantial increase is consistent with the higher fluid transport rates supported by porous emitters. Additional experiments need to be conducted to establish the role of pore size and emitter shape on emission current, specifically the tip radius of curvature, which has been shown to be a relevant parameter in the case of externally wetted emitters [21]. In addition, it has been observed that emission currents increase in a significant way at higher temperature due likely to the reductions of viscosity and the corresponding increase in electric conductivity.

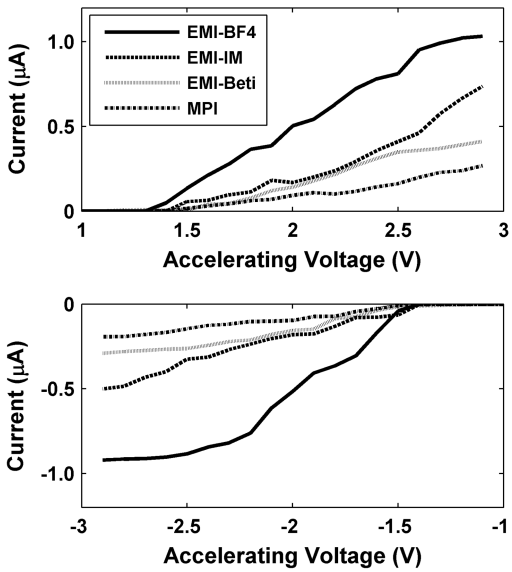

Fig. 8 Emitted current as a function of applied voltage for a single porous metal emitter with 0.5 μm average pore size. Up to 10% variations in current were observed between individual experiments.

B. Significance to Propulsion

The thrust produced by an emitter is equal to the total mass flow rate times the effective ion exhaust velocity. By combining Eq. (2) and (3)

$$T = I_T\sqrt{\frac{2V}{\langle q/m\rangle}} \tag{9}$$

where the mean charge to mass ratio is defined as

$$\langle q/m\rangle = \sum_i f_i\left(\frac{q}{m}\right)_i \tag{10}$$

The thrust increases with a decrease in the mean charge to mass ratio for a fixed acceleration voltage given a steady emitted ion current. However, Fig. 8 shows a clear tendency toward reduced current levels for ionic liquids with heavier ions. Taking the thrust produced by the ionic liquid with the lightest ions, EMI-BF_4, as a reference, and compute the ratio of the thrust of the heavy ionic liquids T_H to that of EMI-BF_4 (T_{BF4}) given the same acceleration voltage, then

Table 5 Summary of emission performance of four different ionic liquids

Ionic liquid	$\langle m \rangle$, amu	$\langle q/m \rangle$, C/g	I, nA	ψ	$\sqrt{\frac{\langle m_{BF_4} \rangle}{\langle m_H \rangle}}$	T^a, μN	I_{SP}, s	η_p
EMI-BF_4	184.38	523.29	695.88	1.00	1.00	0.064	4891	0.929
EMI-IM	362.83	265.92	236.85	0.34	0.71	0.030	3487	0.917
EMI-Beti	544.18	177.30	214.33	0.31	0.58	0.034	2847	0.910
MPI	581.80	165.84	102.13	0.15	0.56	0.017	2754	0.907

[a]At $V = 2200$ V.

$$\frac{T_H}{T_{BF_4}} = \frac{I_H}{I_{BF_4}} \sqrt{\frac{\langle m_H \rangle}{\langle m_{BF_4} \rangle}} \tag{11}$$

Therefore, a heavy liquid will produce more thrust than EMI-BF_4 provided

$$\psi = \frac{I_H}{I_{BF_4}} > \sqrt{\frac{\langle m_{BF_4} \rangle}{\langle m_H \rangle}} \tag{12}$$

The TOF experiments allow us to calculate the mean ion mass being emitted during bipolar operation with both polarities averaged together, the mean charge to mass ratio and the square root of the ion mass ratio. These are shown in Table 5. Taking the measured current magnitudes for each liquid at $V = \pm 2200$ V, the average current for bipolar operation, the current ratio ψ, the thrust and the specific impulse are calculated. It is observed that the porous metal emitters do not emit enough current with heavier ionic liquids to produce more thrust than EMI-BF_4 given the same applied voltage. However, they do operate with lower specific impulses, which could be beneficial in power-limited applications. The reduction in emitted current is caused by the higher viscosity of the heavier ionic liquids and their lower electrical conductivity, causing emission to be limited by fluid flow to the emission region and charge transport. While this phenomenon has been previously studied by varying emitter temperature for externally wetted emitters [14,22], the relative contribution of the viscosity and the conductivity to the observed variations is unknown. It is possible for heavy ionic liquids to emit comparable currents to EMI-BF_4 with a different porosity or at increased temperatures and this is a subject for further work. In summary, the ion mass and emitted current determine the thrust of an electrospray thruster operating in the pure ionic regime. Of these, the current is more relevant than the mass in the overall thrust produced by an electrospray device. On the other hand the specific impulse does not depend on the emitted current, but it does on ion mass. Optimal propellant selection should be carried out by considering the propulsion system as a whole, in the context of a specific application.

V. Performance of Linear Emitter Arrays Fabricated on Porous Metals

Emitter arrays of three different packing densities were fabricated from 0.5 μm porosity Tungsten using the process detailed earlier. Table 6 gives the dimensions of three fabricated emitter arrays, each with a different emitter separation distance and linear emitter density, χ (tips per mm). Figure 9 shows scanning electron microscope images of the emitter arrays. The ionic liquid EMI-BF_4 was used since it was previously shown to produce the most thrust for single emitters. Table 6 also shows the characteristic performance values for each emitter array obtained at the maximum emitted current value achieved, including the net accelerating voltage, the thrust and the specific impulse.

The current per emitter vs applied voltage relationship, displayed in Fig. 10, show that each emitter array produced a maximum current of 1.0–1.5 μA per emitter at the highest applied voltages. The observed spreading of the data is more likely to be attributed to the inevitable variations in the fabrication process as well as differences in emitter aspect ratio rather than a fundamental difference of emission at different densities. Additionally, the emitter to extractor distance was held constant in these tests which means that we could assume that the current would be lower for higher densities (suppressing effect of neighboring emitters on the local electric field) which obscures the results further. This effect leads to a reduced

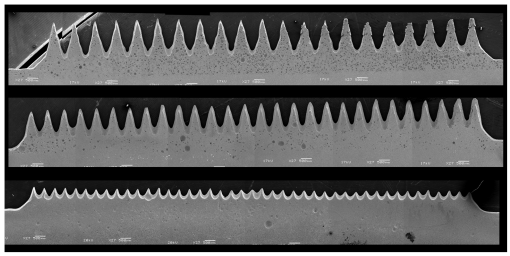

Fig. 9 Linear emitter arrays with different linear packing densities.

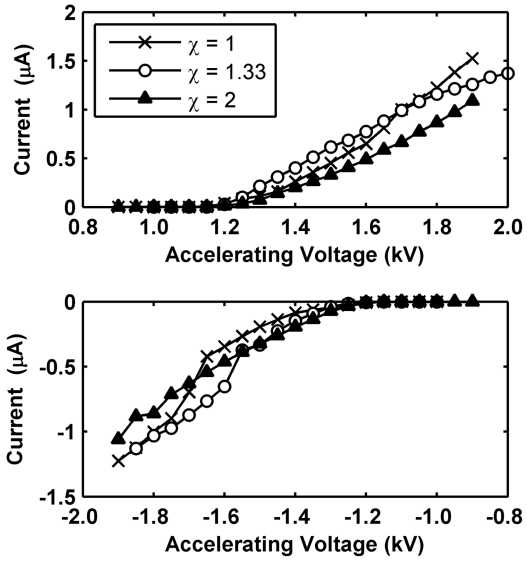

Fig. 10 Emitted current as a function of acceleration voltage.

Table 6 Geometrical properties and performance of linear emitter arrays of various emitter separation distances

Sample #	Emitter length, μm	d, μm	N_E	χ, #/mm	Ia, μA	Va , kV	Ta , μN	I_{SP}a , s
1	1168	958	21	1.00	32.0	1.9	2.8	4500
2	926	730	28	1.33	41.7	2.2	3.9	4850
3	458	500	44	2.00	46.8	1.9	4.0	4500

[a]At max current.

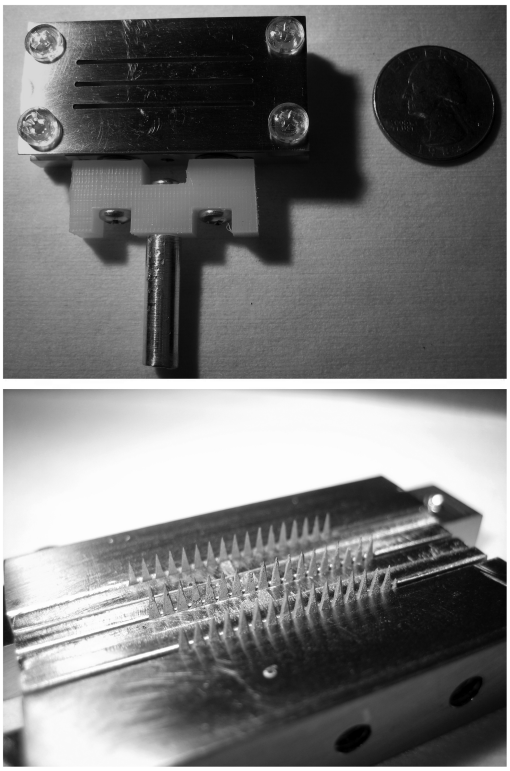

Fig. 11 Two-dimensional emitter array test fixture.

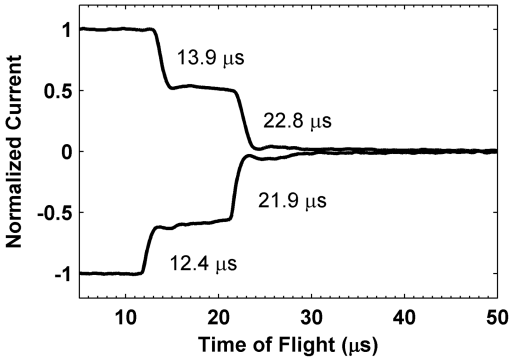

Fig. 12 Time-of-flight response for the two-dimensional emitter array.

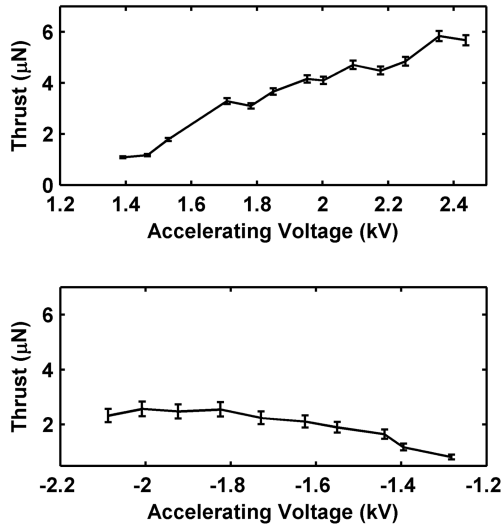

Fig. 13 Measured thrust for positive (top) and negative mode (bottom).

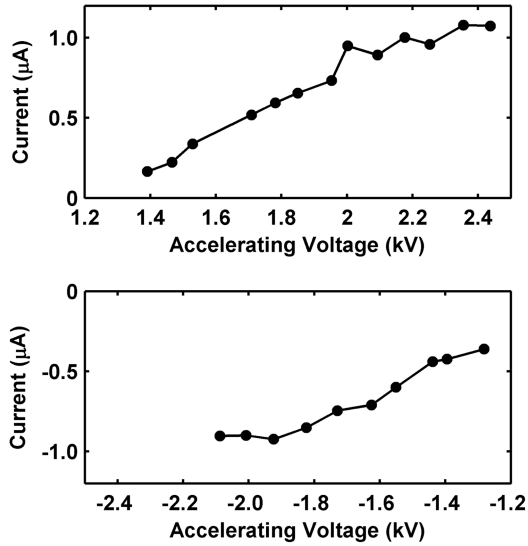

Fig. 14 Measured current per emitter for positive (top) and negative mode (bottom).

electric field at the emitter tips with increasing linear density. The relevant aspect of these results is that the emission current per emitter is not a strong function of emitter density, an important conclusion towards the goal of high-density emitter arrays. Furthermore, fabricating two-dimensional emitter arrays on plane and in a single pass will remove most of the variations in emitter geometry and will allow for photographic scaling and should yield better results.

VI. Two-Dimensional Emitter Arrays

To investigate the performance of loosely packed two-dimensional emitter arrays, a test fixture was created to cluster three linear emitter arrays together. The test fixture was designed to: provide precise alignment between the emitter sheets and the extractor grid to reduce beam impingement; provide adequate insulation (both electrical and fluidic) between the extractor and emitters to reduce the risk of electrical shorting, to use materials which are compatible with ionic liquids; and to allow for easy assembly to reduce the risk of breaking the linear emitter arrays.

The fabricated test fixture (shown in Fig. 11) is an array of 3 flat needle arrays containing 49 working emitters giving an emitter density of a little under 0.5 tips per square mm. The TOF curves for positive ($V = 1915.28$ V) and negative ($V = -1898.33$ V) emission are shown in Fig. 12 while the details of observed ion species are shown in Table 7.

Direct thrust measurements were conducted at the Busek Company, Natick, MA using a torsional balance. The results, plotted in Fig. 13, show that the thruster produced from 0.82–2.33 μN in

Table 7 Properties of the observed ion species

Polarity	Δt, μs	m_i, amu	f	$\langle q/m \rangle$, C/g	Ion species
Positive	13.9	112.40	42.58	430.6	$[EMI]^+$
($V = 1915.28$ V)	22.8	310.15	57.42		$[EMI\text{-}BF_4][EMI]^+$
Negative	12.4	89.49	49.13	513.9	$[BF_4]^-$
($V = -1898.33$ V)	21.9	287.28	50.87		$[EMI\text{-}BF_4][BF_4]^-$

the −1282–−2088 V negative net voltage range and from 1.08–5.67 μN in the 1391–2437 V positive net voltage range. This corresponds to a thrust per emitter tip of 0.048 μN at −2088 V and 0.116 μN at 2437 V. The leveling off of thrust in the negative mode is potentially due to the thruster approaching the limit of its ability to transport liquid to the tip. Additionally, the amount of thrust produced in the negative mode will be less than the positive mode for a given current due to the larger ion charge to mass ratio. The beam current measured on a downstream collector plate and current intercepted by the extractor electrode are shown in Fig. 14. There is a significant amount of intercepted current in this fixture, mostly due to emitter to extractor misalignment caused by mechanical alignment error. Beam interception by electrodes is a serious issue, but one that should be resolvable through precise machining with adequate control of the device geometry.

VII. Conclusions

The electrochemical microfabrication of porous metal electrospray emitters and arrays of emitters and their characterization are discussed in this work. Single emitters are tested with ionic liquids with various physical properties, specifically dissimilar ion masses. These tests confirm that porous emitters operate in the pure ionic regime and are therefore capable of high-efficiency operation in a wide range of specific impulses. The thrust increase expected from emitting massive ions is overwhelmed by the reduction in current likely caused by limited fluid transport through the emitter to the emission region at a given temperature. Emitters are also studied in linear arrays of varying emitter spacing and length. It is shown that the amount of ionic current emitted by the different linear arrays is roughly constant suggesting that clustering does not have a significant effect on the amount of current, and therefore thrust, from each emitter. This allows the thrust density of electrospray emitter arrays to be greatly increased with emitter and array miniaturization.

Lastly, a macroscale two-dimensional array of emitters is fabricated by combining three linear emitter arrays together in a test fixture. Current measurements indicate that the array produce around 1 μA/emitter at the higher voltages in both polarities, however, there is a significant amount of current intercepted by the extractor. This is likely caused by the difficulty of mechanically aligning the emitters and extractor. This issue would be mitigated in a fully microfabricated device. Direct thrust measurements show that the device produce thrust in both polarities, but in the negative polarity the thrust levels off at higher voltages. This could be caused by the effect of fluid transport to the emitter region and the increase in the amount of current intercepted by the extractor. Further tests will need to be conducted with better aligned devices and emitters with different pore size and perhaps increased temperatures. The next step in this area is to create two-dimensional emitter arrays from a single wafer thus simplifying alignment and increasing overall compactness.

The results of these initial tests with porous metal electrospray emitters show that this technology would be an attractive solution to a number of space propulsion needs. This high specific impulse technology can be easily scaled from thrust levels in the sub μN level to well over 1 mN and is therefore suitable for a wide variety of missions from pico/nano satellites to larger standard satellites. With further miniaturization, electrospray thrusters become competitive with conventional electric propulsion technologies in terms of mass, area and volume for a given amount of thrust and should be adequate to create thruster panels that would scale in a similar way to solar panels for a variety of missions.

Acknowledgments

The funding for this work was provided by an AFOSR YIP Award monitored by Mitat Birkan and the Massachusetts Institute of Technology Karl Chang Innovation Fund. We are thankful to F. de la Mora for his generous contribution of the EMI-Beti and MPI ionic liquids. Also special thanks to Busek Co Inc for performing the thrust measurements.

References

[1] Taylor, G. I., "Disintegration of Water Drops in an Electric Field," *Proceedings of the Royal Society of London, Series A: Mathematical and Physical Sciences*, Vol. 280, No. 1382, pp. 383–397. doi:10.1098/rspa.1964.0151

[2] Romero–Sanz, I., Bocanegra, R., Fernandez de La Mora, J., and Gamero–Castano, M., "Source of Heavy Molecular Ions Based on Taylor Cones of Ionic Liquids Operating in the Pure Ion Evaporation Regime," *Journal of Applied Physics*, Vol. 94, No. 5, 2003, pp. 3599–3605. doi:10.1063/1.1598281

[3] Cohen, E., Somol, C. J., and Gordon, D. A., "A 100 kV, 10-W Heavy Particle Thruster," AIAA Paper 65-377, 1965.

[4] Kidd, P. W., and Shelton, H., "Life Test (4350 Hours) of an Advanced Colloid Thruster Module," *10th AIAA Electric Propulsion Conference*, AIAA, New York, Oct. 1973.

[5] Lozano, P., and Martinez-Sanchez, M., "Ionic Liquid Ion Sources: Characterization of Externally Wetted Emitters," *Journal of Colloid and Interface Science*, Vol. 282, No. 2, 2005, pp. 415–421. doi:10.1016/j.jcis.2004.08.132

[6] Castro, S., Larriba, C., , Fernandez de la Mora, J., Lozano, P., Sumer, S., Yoshida, Y., and Saito, G., "Effect of Liquid Properties on Electrosprays from Externally Wetted Ionic Liquid Ion Sources," *Journal of Applied Physics*, Vol. 102, No. 9, Nov. 2007, pp. 094310–094315. doi:10.1063/1.2802547

[7] Larriba, C., Castro, S., de la Mora, J. F., and Lozano, P., "Monoenergetic Source of Kilodalton Ions from Taylor Cones of Ionic Liquids," *Journal of Applied Physics*, Vol. 101, No. 8, April 2007, pp. 084303–084306. doi:10.1063/1.2717858

[8] Gassend, B., Velasquez-Garcia, L. F., Akinwande, A. I., and Martinez–Sanchez, M., "A Microfabricated Planar Electrospray Array Ionic Liquid Ion Source with Integrated Extractor," *Journal of Microelectromechanical Systems*, Vol. 18, No. 3, June 2009, pp. 679–94. doi:10.1109/JMEMS.2009.2015475

[9] Courtney, D. G., Li, H., Maqueo, P. D. G., Fedkiw, T., and Lozano, P. "On the Validation of Porous Nickel as Substrate Material for Electrospray Ion Propulsion," *46th AIAA/ASME/SAE/ASEE Joint Propulsion Conference and Exhibit*, Paper 2010-7020, July 2010.

[10] Khyams, V., "Advanced Propulsion for Microsatellites," MIT Doctoral Thesis, Massachusetts Inst. of Technology, 2000.

[11] Legge, R., and Lozano, P., "Method and Apparatus for a Porous Metal Electrospray Emitter," International Patent, Publication Number WO-2009/137583-A2, Nov. 2009.

[12] Williams, K. R., Gupta, K., and Wasilik, M., "Etch Rates for Micromachining Processes: Part II," *Journal of Microelectromechanical Systems*, Vol. 12, No. 6, Dec. 2003, pp. 761–778. doi:10.1109/JMEMS.2003.820936

[13] Lozano, P., and Martínez-Sánchez, M., "Ionic Liquid Ion Sources: Suppression of Electrochemical Reactions Using Voltage Alternation," *Journal of Colloid and Interface Science*, Vol. 280, No. 1, 2004, pp. 149–154. doi:10.1016/j.jcis.2004.07.037

[14] Lozano, P., and Martinez–Sanchez, M., "Ionic Liquid Ion Sources: Characterization of Externally Wetted Emitters," *Journal of Colloid and Interface Science*, Vol. 282, No. 2, 2005, pp. 415–421. doi:10.1016/j.jcis.2004.08.132

[15] Lozano, P., "Energy Properties of an EMI-Im Ionic Liquid Ion Source," *Journal of Physics D: Applied Physics*, Vol. 39, No. 1, Jan. 2006, pp. 126–134. doi:10.1088/0022-3727/39/1/020

[16] Gamero–Castano, M., "A Torsional Balance for the Characterization of Micro Newton Thrusters," *Review of Scientific Instruments*, Vol. 74, No. 10, Oct. 2003, pp. 4514–4519. doi:10.1063/1.1611614

[17] Lozano, P., and Martinez-Sanchez, M., "Efficiency Estimation of EMI-BF4 Ionic Liquid Electrospray Thrusters," AIAA 2005-4388, July 2005.

[18] Garoz, D., Bueno, C., Larriba, C., Castro, S., Romero–Sanz, I., Fernandez de la Mora, J., Yoshida, Y., and Saito, G., "Taylor Cones of Ionic Liquids from Capillary Tubes as Sources of Pure Ions: The Role of Surface Tension and Electrical Conductivity," *Journal of Applied Physics*, Vol. 102, No. 6, Sept. 2007, pp. 064913–064923. doi:10.1063/1.2783769

[19] McEwen, A. B., Ngo, H. L., Lecompte, K., and Goldman, J. L., "Electrochemical Properties of Imidazolium Salt Electrolytes for Electrochemical Capacitor Applications," *Journal of the Electrochemical Society*, Vol. 146, No. 5, 1999, pp. 1687–1695. doi:10.1149/1.1391827

[20] Lozano, P., Gassend, B., and Martinez-Sanchez, M., "Performance Characteristics of a Linear Ionic Liquid Electrospray Thruster," International Electric Propulsion Conference IEPC-2005-192, 2005.

[21] Castro, S., and de la Mora, J. F., "Effect of Tip Curvature on Ionic Emissions from Taylor Cones of Ionic Liquids from Externally Wetted Tungsten Tips," *Journal of Applied Physics*, Vol. 105, No. 3, 2009, pp. 034903–04908.
doi:10.1016/j.jcis.2004.08.132

[22] Higuera, F. J., "Model of the Meniscus of an Ionic–Liquid Ion Source," *Physical Review E (Statistical Physics, Plasmas, Fluids, and Related Interdisciplinary Topics)*, Vol. 77, No. 2, 2008, pp. 1–11.
doi:10.1103/PhysRevE.77.026308

A. Gallimore
Associate Editor